UDC 544.032.4

DOI: 10.15372/CSD2024614

EDN: ACVJDU

Evaluation of Thermal Degradation Parameters of Polyaniline-Based Bismuth Telluride Nanocomposites

A. V. ZHMUROVA[1], B. A. LOGINOV[2], M. V. ZVEREVA[1]

[1]*A. E. Favorsky Irkutsk Institute of Chemistry, Siberian Branch of the Russian Academy of Sciences, Irkutsk, Russia*

E-mail: anna-zhmurova@irioch.irk.ru

[2]*National Research University of Electronic Technology, Moscow, Russia*

(Received 02.09.2024; accepted 25.09.2024)

Abstract

The effect of bismuth telluride (Bi_2Te_3) nanoparticles and multi-walled carbon nanotubes (MWCNTs) on thermal destruction and surface morphology of their nanocomposites with polyaniline (PANI) at different nanophase contents (Bi_2Te_3 – 7.3 wt%, MWCNTs – 1.5 wt%), obtained for the first time using the mechanochemical approach, has been investigated. It is shown on the basis of the data obtained by simultaneous thermal analysis and scanning tunnelling microscopy that the introduction of inorganic nanophase has a key effect on the thermal properties of the synthesised composites PANI–Bi_2Te_3 and PANI–Bi_2Te_3–MWCNTs, as well as on their structure. The thermal stability of nanocomposites and the initial polymeric matrix, assessed from the temperature of the onset of the second mass loss stage, is the same and equal to 166 °C.

Keywords: polyaniline, bismuth telluride, carbon nanotubes, nanoparticles, nanocomposites, thermal destruction

INTRODUCTION

The concept of sustainable consumption of energy resources reflects in energy-saving systems, in particular in the devices combining the functions of thermoelectric generators and thermoelectric coolers [1]. The transformation of thermal energy released during the operation of energy-consuming devices (lasers, capacitors, processors, etc.) into electricity allows the latter to be accumulated in energy storage devices and be used later on for feeding the same devices. Development of the components for energy saving in autonomous technical systems is of special interest. The devices containing thermoelectric generators and used in wearable electronic systems can be the examples of such components [2, 3]. These generators and thermoelectric materials used in them often possess definite flexibility, which can be provided either by a specially chosen substrate [4] or by the particular characteristics of the thermoelectric matrix, which is polymeric in its nature, as a rule [5]. In this respect, the systems of special interest are polymer-inorganic ones [6], including nanocomposites with nanophase bismuth telluride (Bi_2Te_3) [7]. The application of inorganic thermoelectrics, known for their excellent ability to transform the energy, as the nano-sized component of organic-inorganic thermoelectrics allows obtaining the composites with a rather high thermoelectric figure of merit for the structures of this class [8]. It is important to use conducting polymers as a matrix incorporated in thermoelectrics [9]. A representative of the group of these polymers is polyaniline (PANI) [10]. Conducting polymers can provide the necessary

electrical conductivity of the material, so they are extensively used as a component of multiphase nanocomposite systems [11]. Carbon materials can be also used for this purpose [12], for example, multi-walled carbon nanotubes (MWCNTs). They are used both as an individual dopant in nanocomposites [13, 14] and as a component in complex polymer-inorganic systems [12].

We have previously successfully synthesized PANI–Bi_2Te_3 and PANI–Bi_2Te_3–MWCNTs nanocomposites using environmentally friendly and available mechanosynthesis, studied their electrical conductivity depending on temperature [15]. For the materials to be used at heating in the air, an essential parameter is thermal stability, that is, stability against thermal destruction, because the loss of structural integrity causes changes in the physical properties inherent to these materials. Research publications deal with the data on the thermal destruction of PANI [16–18], its nanocomposites with nanoparticles γ-Al_2O_3 [16], Ag–Cu_2O [19], Ni [20], Ag [18] and other particles, but thermal destruction of PANI–Bi_2Te_3 and PANI–Bi_2Te_3–MWCNTs nanocomposites has not been studied previously.

To reveal the morphological features of the nanophase, transmission electron microscopy (TEM) is traditionally used, which has become the gold standard in material characterisation, along with scanning electron microscopy (SEM). In addition, essential information on the surface properties of materials can be obtained by scanning tunnelling microscopy (STM) [21]. The data obtained using STM are also of interest from the practical viewpoint because, for example, solid-phase polymer-inorganic nanocomposites are often used in the pressed or moulded forms. These materials are used as the components of technical devices that are to be conjugated with each other, and it is necessary to determine the structural features of the obtained surface in this case. This method is extensively used to analyse the structure of carbon nanomaterials [22, 23], as well as multiphase polymer-inorganic nanocomposites containing MWCNTs [24].

The goal of the present work was to study the effect of the inorganic nanophase on thermal destruction of PANI–Bi_2Te_3 and PANI–Bi_2Te_3–MWCNTs nanocomposites synthesised mechanochemically, and to investigate the features of the morphology of pressed samples depending on their composition.

EXPERIMENTAL

Materials

Aniline (RM-Engineering, Russia) was distilled in vacuum in the inert atmosphere prior to use. Sodium persulphate (Reachim, Russia), HCl of specially pure grade (Sigma-Tek, Russia), polyethylene glycol (PEG-400, Merck, Germany), powdered tellurium (Alfa Aesar, USA), bismuth nitrate pendahydrate (NPF Nevskiy Khimik, Russia), ethanol (Konstanta-Farm, Russia), NaOH (Reachim, Russia), hydrazine hydrate (Vekton, Russia) and multiwalled carbon nanotubes (MWCNTs, Suzhou Tanfeng Graphene Technology Co., China) were used without additional purification. Dialysis bag (Scienova GmbH, Germany) with a pore diameter of 3.5 kDa was used for dialysis.

Methods of investigation

The infrared (IR) spectra of samples prepared as tablets with KBr were recorded within the wavenumber range 4000–400 cm^{-1} using an IR Fourier spectrometer 3100 FT IR (Varian, USA) according to the procedure described in detail in [15]. Powder X-ray diffraction (XRD) analysis was carried out using a D8 ADVANCE diffractometer (Bruker, Germany) equipped with a Goebel mirror, with CuK_α-radiation in the Locked Coupled mode, with 1 s exposure. The elemental composition was determined by X-ray energy-dispersive microprobe analysis using a scanning electron microscope TM 3000 (Hitachi, Japan) with an X-ray detector SDD XFlash 430-4 and using a CHNS-analyser Flash 2000 (Thermo Fisher Scientific, USA).

Simultaneous thermal analysis (STA) of the samples was carried out using a STA449F1 Jupiter thermal analyser (Netzsch, Germany), at the heating rate of 10 °C/min in the air. Heating was carried out within the temperature range 27–1000 °C in corundum crucibles for differential scanning calorimetry (DSC). The volatile products of reactions proceeding during thermal destruction of the samples were detected with a QMS403C Aeolos mass spectrometer (Netzsch, Germany), connected to the thermoanalyser through a quartz capillary 75 μm in diameter, encapsulated in a shell made of stainless steel. The feedline was well insulated and heated to 200 °C to prevent the condensation of gases. The voltage at the electron ionisation source in the mass spectrom-

eter was 70 eV, the ions were recorded with a secondary electron multiplier. Experiments were carried out multiply to test the reproducibility of the obtained experimental values. The data presented in the work are averaged. The STA method combines thermogravimetry (TG), DSC and mass spectrometry of volatile products. The mass loss (%) was calculated from TG curves taking the initial sample mass as 100 %. The mass change derivative with respect to the temperature is designated as the differential thermogravimetry (DTG) curve.

To investigate the surface morphology, the samples of PANI and PANI–Bi_2Te_3, PANI–Bi_2Te_3–MWCNTs nanocomposites were pressed into tablets of 11 mm in diameter, 1 mm thick. The images of tablet surfaces in STM mode were obtained using a scanning probe microscope SMM-2000 (PROTON, Russia, No. 46918 in the State Registry of Measuring Equipment of the Russian Federation). STM-frames 1.117 × 1.117 μm and 558.3 × 558.3 nm in size were obtained by scanning the surface of tablets.

Procedure for PANI synthesis in the form of emeraldine salt

The synthesis of PANI in its electrically conducting form was performed according to the procedure described in detail in [15] with insignificant amendments. Freshly distilled aniline in the amount of 4.56 mL was added to 50 mL of a 1 M HCl solution. After thermostating the reaction mixture for 30 min at 5 °C, 20 mL of a 2.4 M aqueous solution of $Na_2S_2O_8$ was added slowly, drop by drop, while stirring. The reaction was conducted at 3–5 °C for 6 h. After the indicated time, the dark-green reaction mixture was subjected to dialysis with respect to distilled water for 12 h to remove residual inorganic reagents and the products of their reaction. Then the formed polymer was filtered off using a Schott filter, with subsequent multiple washing with water and ethanol, dried in the air at room temperature. The yield was 93.2 %. The product contains, wt%: C 55.61; H 4.20; N 9.33. No ash is formed.

Synthesis of Bi_2Te_3 nanoparticles stabilised with polyethylene glycol (PEG-400)

In a three-necked flask, 6.2 mL of $N_2H_4 \cdot H_2O$ was added to 2.5 g of NaOH. While stirring, the reaction mixture was heated to 70 °C. Then the reaction mixture was bubbled with argon, 4 g of powdered tellurium was added, and the mixture was kept for 30 min under intense stirring in the inert atmosphere until the complete dissolution of tellurium. The obtained bluish-violet mixture contained Te^{2-} ions. Then the mixture was added to a solution of $Bi(NO_3)_3 \cdot 5H_2O$ in ethylene glycol (EG) (10.43 g in 30 mL of EG), and then 9.38 mL of polyethylene glycol (PEG-400) was added to the resulting black mixture. Thus obtained pegylated Bi_2Te_3 nanoparticles were thermostated at 30 °C in argon for 20 min, after which the formed Bi_2Te_3 nanoparticles were separated by centrifuging (3000 r.p.m., 15 °C, 7 min) and multiple washing of the precipitate with water to neutral pH. The yield of Bi_2Te_3 nanoparticles was 41.2 %. Analysis data, wt%: C 1.00; H 2.32; ash 96.68.

Procedure of the mechanochemical synthesis of PANI–Bi_2Te_3 nanocomposite

A mixture of PANI powder (4.8 g) and Bi_2Te_3 nanoparticles (1.2 g) was subjected to treatment for 60 min in a ball mill ML-1 (NPEF Ekon, Russia) with the working chamber made of titanium. After mechanochemical treatment, 5.65 g of PANI–Bi_2Te_3 composite was unloaded, which corresponds to the yield equal to 94 %. Analysis data, wt%: C 42.28; H 3.63; N 7.83; ash 20.55.

Procedure for obtaining PANI–Bi_2Te_3–MWCNTs nanocomposite

A mixture of PANI (4.8 g), Bi_2Te_3 nanoparticles (1.2 g) and MWCNTs (0.09 g) was placed in the ML-1 ball mill and subjected to treatment for 60 min. The yield of PANI–Bi_2Te_3–MWCNTs was 96–98 %. Analysis data, wt%: C 41.40; H 3.47; N 7.55; ash 20.40.

RESULTS AND DISCUSSION

A detailed description of the synthesis process and the structure of initial electrically conducting salt of PANI, as well as the Bi_2Te_3-containing composite based on PANI was presented elsewhere [15]. In the present work, we studied the features of thermal destruction in the air, thermal stability parameters of the obtained nanocomposites PANI–Bi_2Te_3 and PANI–Bi_2Te_3–MWCNTs, and the effect of the nanosized Bi_2Te_3 phase and MWCNTs on the specific features of the surface structure of pressed PANI, PANI–Bi_2Te_3 and PANI–Bi_2Te_3–MWCNTs. The object of investiga-

tion was PANI sample in its electrically conducting form: emeraldine salt. According to the IR spectroscopic data (Fig. 1, *a*), the spectrum of initial PANI is characterised by a set of absorption bands (a. b.) in the region of 500–4000 cm^{-1}. The a. b. determined in the spectrum relate to the stretching vibrations of C=C bonds of quinondiimine fragments at 1577 cm^{-1} and C–C phenylene diamine fragments at 1492 cm^{-1}; to the vibrations of $C_{benzene}$–N=$C_{quinoid}$ bonds and the bending vibrations of C–N bonds at 1374 and 1299 cm^{-1}, respectively; to the stretching vibrations of $C–N^+$ polaron structures at 1243 and 1134 cm^{-1}; to the in-plane bending vibrations of C–H bonds in benzenoid rings as a shoulder at 1043 cm^{-1} and out-of-plane stretching vibrations of C–H bonds in benzenoid rings at 818 cm^{-1} [15]. An intense a. b. at 3422–3424 cm^{-1} is most probably due to the presence of adsorbed water molecules in KBr using for sample preparation. The introduction of Bi_2Te_3 nanoparticles into the polymer PANI matrix as a result of mechanochemical activation is accompanied by retaining the a. b. observed for polyaniline.

According to XRD data (see Fig. 1, *b*), the average size of nanophase crystals in the synthesised PANI–Bi_2Te_3 nanocomposite, calculated according to the Scherrer equation, is 17.0 nm. The diffraction pattern of PANI–Bi_2Te_3 nanocomposite is characterised by the presence of a number of reflections with different intensities, corresponding to (101), (015), (1010), (110), (0015), (205), (0210) and (1115) planes of the rhombohedral lattice of bismuth telluride, which, in turn, is in good agreement with the diffraction pattern of standard bismuth telluride samples (JCPDS 15-0863).

Thermal analysis of PANI samples has been represented in detail in [16–18]. According to the results of these works, thermal destruction of PANI can proceed in two or three stages. A three-stage thermal destruction of the PANI–HCl salt system was observed in [17]: mass loss (5–6 %) up to 110 °C corresponds to the first stage of decomposition due to water evaporation, a decrease in mass (4 %) within the range of 110–310 °C at the second stage is due to simultaneous bound water evaporation and de-doping process (HCl removal); the largest mass loss at the third (main) stage relates to the oxidative destruction of the doped polymer. The destruction of PANI can be completed in the region near 600 °C [17]. A two-stage destruction of PANI–HCl was observed in [16]. The first stage of thermal destruction, associated with water evaporation and leading to 8 % mass loss by PANI, was observed at 90 °C, while massive destruction of the polymer proceeds in the region of 200–620 °C, with the minimum on the DTG curve at 400 °C. After polymer destruction is completed at 620 °C, the sample mass remained unchanged and accounted for 2.3 % of the initial value. A three-stage destruction of PANI was observed in [18]. According to DSC data described in [18], water removal from PANI proceeded up to 100 °C. The next stage of thermal decomposition, involving the destruction of monomers with small molecular mass and de-doping process, was observed as a shoulder on the DSC curve within temperature range 250–300 °C. The main destruction, followed by PANI melting, was depicted on the DSC curve as the exothermal peak at 380.3 °C and the endothermic peak at 495.7 °C, respectively.

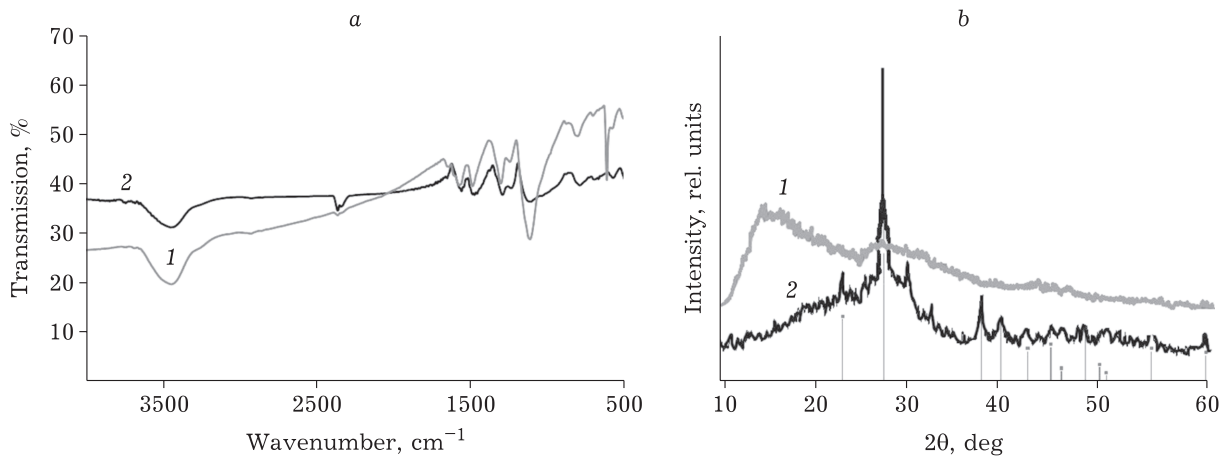

Fig. 1. IR spectra (*a*) and XRD patterns (*b*) of polyaniline (PANI) (*1*) and the PANI–Bi_2Te_3 nanocomposite (*2*).

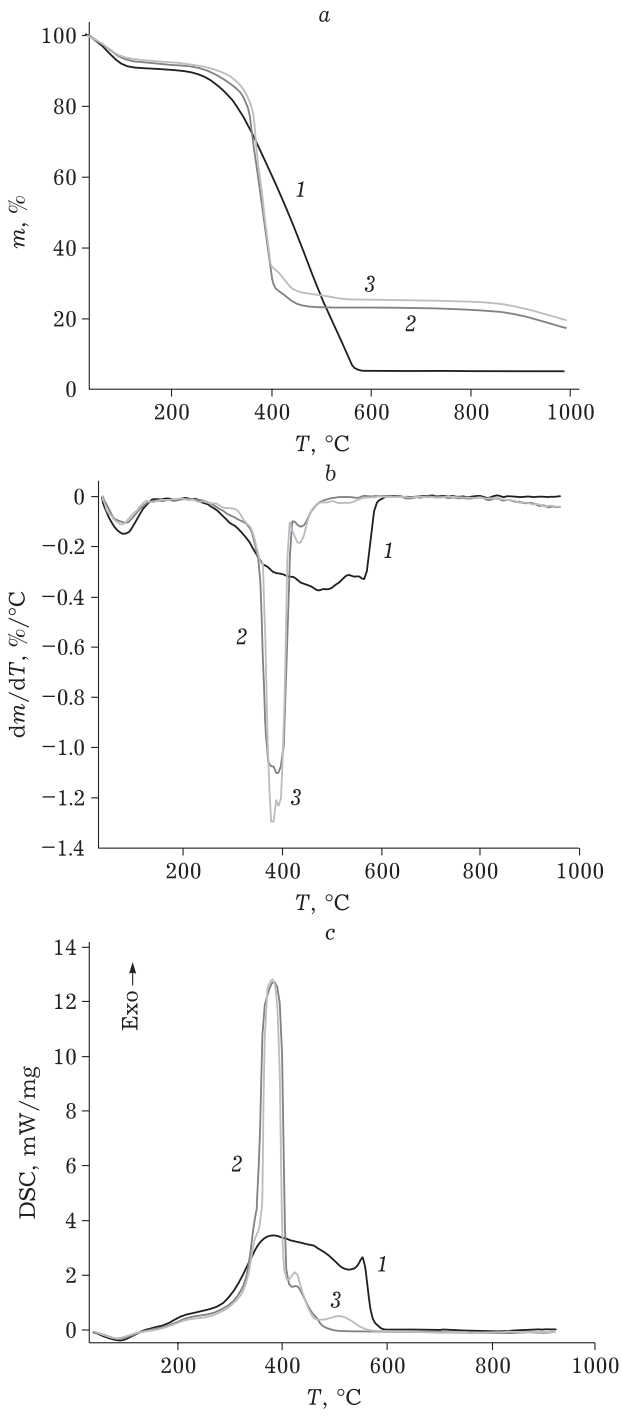

Fig. 2. Results of the studies of samples: PANI (*1*), PANI–Bi_2Te_3 (*2*) and PANI–Bi_2Te_3–MWCNTs (*3*) using the methods: *a* – thermogravimetry (TG), *b* – differential thermogravimetry (DTG), *c* – differential scanning calorimetry (DSC). Here and in Fig. 3: PANI – polyaniline; MWCNTs – multi-walled carbon nanotubes; *m* – mass, %; *T* – temperature, °C.

The major regularities of the thermal destruction of PANI, obtained in the present investigation, are in good agreement with the previously published data [18].

The thermograms and the DTG and DSC curves of PANI, PANI–Bi_2Te_3 and PANI–Bi_2Te_3–MWCNTs samples are shown in Fig. 2. According to STA data, thermal destruction of the synthesised PANI sample in the form of its emeraldine salt proceeds in three stages. Water removal, detected within the temperature range 27–141 °C with the minimum on DTG curve at 79.5 °C causes 9 % mass loss. The second stage of destruction is represented on the DSC curve by the exothermal shoulder at 166–219 °C, and on the DTG curve by a scarcely noticeable minimum within this temperature range. Mass loss was 0.6 %. The mass spectra of the second stage of destruction exhibit prevailing release of the species with mass numbers 28–38, corresponding, most probably, to the products of polymer de-doping and its partial depolymerisation (removal of HCl and low molecular weight monomers). The third stage of the thermal destruction of PANI, corresponding to the largest mass loss by the sample, starts at 219 °C and ends at 577 °C. After this stage, the residual mass is conserved at a level of 5 %, in spite of further heating (see Fig. 2, *a*). This stage of polymer destruction is a consequence of complex decomposition processes, represented on the DTG curve by overlapping bands with shoulders at 287, 371 °C and minima at 470, 547 °C (see Fig. 2, *b*). These thermal processes are observed on the DSC curve (see Fig. 2, *c*) as exothermal maximums at 377, 460 °C and an endothermic minimum at 530 °C. The shoulder at 287 °C on the DTG curve corresponds to the release of substances mainly with mass numbers 35 (Cl^-), 41 (C_2H_3N from aromatic *N*-methyl-heterocycles). The exothermal effect at 460 °C corresponds to the release of the products of thermal decomposition of PANI characterised by a set of maxima with mass numbers 30–32. Mass loss at the third stage of polymer destruction was 84.7 %.

The introduction of Bi_2Te_3 nanoparticles into PANI has a crucial effect on thermal destruction processes. The first stage of decomposition, namely water evaporation, is identified within the temperature range 27–121 °C with a minimum on the DTG curve at 78 °C and endothermic effect at 87 °C on the DSC curve. Completion of water removal from the nanocomposite is observed at a lower temperature in comparison with the matrix, which may be due to more intense water evaporation as a consequence of the difference in the specific heat values between nanophase and the matrix. The loss of nanocomposite sample mass (7.1 %) is smaller in comparison with PANI (9 %). A decrease in this pa-

rameter with the addition of nanoparticles was previously observed in some polymer-inorganic nanocomposites [25, 26]. This effect is likely to be associated with the lower hygroscopicity of the nanocomposite in comparison with the polymeric matrix. The second stage of destruction manifests itself on TG and DTG curves in the region of 166–230 °C, it is represented on the DSC curve by the exothermal shoulder at 220 °C. Mass loss was 0.8 %. The third stage of destruction, corresponding to the largest mass loss by the nanocomposite PANI–Bi_2Te_3 (68 %), starts somewhat later (230 °C) than for the polymeric matrix, and ends at 487 °C. The destruction of nanocomposite is likely to proceed in four stages: on the DTG curve, one may see a shoulder at 289 °C, two overlapping minimums at 364 and 379 °C, mass loss at 426 °C. On the DSC curve, these processes correspond to a shoulder at 345 °C, two exothermal effects at 368 and 385 °C, and exothermal effect at 428 °C. According to the mass spectra, the release of volatile reaction products with mass numbers 15–35 is observed at the third stage of destruction. The introduction of nanoparticles into PANI leads to the emergence of the fourth stage of thermal destruction, starting at 779.3 °C and ending outside the measurement area (>977 °C), with a clear minimum at 937.4 °C on the DTG curve. A weak exothermal effect is detected on the DSC curve at 937 °C. This stage is likely to be connected with nanophase Bi_2Te_3 melting. The loss of nanocomposite mass, observed in this experiment at the last stage, was 6.4 %.

The first stage of PANI–Bi_2Te_3–MWCNTs nanocomposite decomposition was determined to proceed within the temperature range 27–122 °C, with the minimum on DTG curve at 73.4 °C. This stage manifests itself on the DSC curve as the endothermic peak at 80 °C. The mass loss at the first stage of decomposition is 6.4 %. The second stage of decomposition is observed within the temperature range 166–240 °C as a shoulder on the DSC curve at 206 °C. Mass loss is 1.1 %. The third (main) stage of nanocomposite destruction, detected within the range 240–572 °C, is evidence of a number of destructive processes: on the DTG curve, there are a shoulder at 347 °C; overlapping minimums at 369.2 and 382.1 °C, and the effects observed at 422 and 509.8 °C. These processes are also represented on the DSC curve as an exothermal shoulder at 347 °C, overlapping exothermal effects at 372.2 and 381.3 °C, maxima at 424.5 and 509.0 °C. It should be stressed that the presence of MWCNTs in the nanocomposite has caused the appearance of exothermal effect at 509.0 °C, which is absent in the STA data of PANI–Bi_2Te_3 nanocomposite. According to the data of mass spectroscopy, the third stage of destruction involves the release of compounds with mass numbers 15–41. The mass loss at the third stage is 66.4 %. The fourth stage of PANI–Bi_2Te_3–MWCNTs decomposition proceeds similarly to PANI–Bi_2Te_3 within the temperature range 779.3–977.0 °C. However, the corresponding minimum on the DTG curve (see Fig. 2, *b*) is likely to occur at a higher temperature than 977.0 °C (out of the temperature range for this experiment). Mass loss at this stage is 6.3 %.

As shown in [27], the thermograms of PANI and PANI–MWCNTs only insignificantly differ from each other in the duration of the main destruction stage and in the shape. In this respect, it appears logical to assume that the addition of MWCNTs to PANI–Bi_2Te_3 would not lead to substantial differences in their thermograms. Maybe, for this reason the thermograms of PANI–Bi_2Te_3 and PANI–Bi_2Te_3–MWCNTs are almost identical and differ substantially from the STA data for PANI. However, it is necessary to note that the introduction of MWCNTs into PANI–Bi_2Te_3 nanocomposite causes much more rapid destruction of the nanocomposite in the region of 369 °C, the appearance of destruction process at 509 °C, the change of the fourth stage of destruction, an increase in the residual mass, which is also characteristic of nanocomposites containing only MWCNTs as the nanophase [28, 29].

The TG data give information on the parameters characterising thermal stability of the samples. As a rule, thermal stability is determined as the temperature corresponding to the onset of destruction stage following the stage related to water removal (T_{oII}). A convenient parameter of thermal stability is also the temperature corresponding to the highest mass loss rate (T_m). At the same time, thermal stability is calculated as the temperature of a definite degree of mass loss during destruction, mainly 5, 10, 30, 50 % (T_5, T_{10}, T_{30}, T_{50}, respectively) [30]. The information on thermal stability can also be obtained from such parameters determined from TG data as the residual mass, and by calculating the heat resistance index (T_{HRI}) according to equation [31]:

$$T_{HRI} = 0.49(T_5 + 0.6(T_{30} - T_5))$$

The calculated parameters of PANI thermal stability are shown in Fig. 1. One can see that the initial destruction of PANI and nanocomposites occurs at a temperature higher than 166.0 °C, in-

dependently of the presence of type of nanophase. At the same time, the temperature corresponding to the largest mass loss decreases from 470.0 to 379.0 °C after the introduction of nanoparticles into PANI, while after the addition of MWCNTs it drops to 368.7 °C. With the addition of Bi_2Te_3 nanoparticles, the parameters T_5 and T_{10} increase from 81.0 to 88.0 °C and from 228.2 to 272.3 °C, respectively. The introduction of MWCNTs into the nanocomposite also leads to further increase in T_5 and T_{10} to 91.5 and 292.9 °C, respectively. A different situation is observed for T_{30} and T_{50}. The presence of Bi_2Te_3 nanoparticles causes a decrease in T_{30} from 370.0 (for PANI) to 360.1 °C, and T_{50} from 433.4 to 379.3 °C. The presence of MWCNTs in the system causes a slight increase in these parameters, however, they do not reach the values corresponding to PANI: T_{30} increases to 366.0 °C, and T_{50} to 381.5 °C. In the presence of Bi_2Te_3 nanoparticles, a decrease in T_{HRI} from 124.7 to 123.1 °C is indicative, while after the addition of MWCNTs this parameter becomes higher (125.5 °C) than the value determined for PANI. The residual mass increases with the introduction of Bi_2Te_3 (and with the addition of MWCNTs), reaching 18.6 %. The observed changes of thermal stability parameters occur as a consequence of different nature and rates of destruction processes for PANI and nanocomposites, which is associated with their composition.

The STM images of PANI and nanocomposites (PANI–Bi_2Te_3 and PANI–Bi_2Te_3–MWCNTs) are shown in Fig. 3. The structure of the sample surface is directly dependent on sample composition (see Fig. 3, *a*, *d*). Thus, the structure of the PANI surface is formed by randomly distributed polymer molecules. The structure is rather uniform, there are no significant depressions and hills. The height difference between the deepest depression and the highest hill is not large, it is only 31.7 nm. The structure of the PANI–Bi_2Te_3 nanocomposite surface is radically different (see Fig. 3, *b*, *e*). The height difference between the deepest depression and the highest hill is substantial (58.2 nm). A specific feature of the surface structure of this sample is the presence of clearly visualised two types of hills. The hills of the first type are 37.0 nm high; they possess larger area and arbitrary shapes. These hills have sloping surfaces with height difference between the extreme points of the slope equal to 23.0 nm. These regions of the STM frame is likely to show the surface under which the nanophase is absent along a definite distance, and PANI is located closer to the surface. The second type of hills possesses smaller area, and the shape is close to spherical. The diameter of these grains varies from 40.0 to 476.0 nm, while the height varies from 19.0 to 58.2 nm. The hills of the second type can be Bi_2Te_3–PANI nanoparticles with the core-shell structure, located either close to the surface or at a definite depth but clearly observable under PANI layer. The structure of PANI–Bi_2Te_3–MWCNTs nanocomposite surface is substantially different from other samples (Fig. 3, *c*, *f*). The maximum difference in surface height was 44.8 nm. Three quasi-regular systems of different directionality are clearly observed in the STM frame (see Fig. 3, *c*). Each system is represented by almost parallel extended heights of different thickness. The system observed in the lower part of the frame is formed by three hills with sloping edges, similar in height (10.0–12.0 nm), length (443.0 nm) and width (121.0–173.0 nm). These structures spring from the left lower corner, elevate to the right upper one and end abruptly in their upper part. This system may be a rather deepened group of MWCNTs, so that the morphological features of MWCNTs are not visible in its surroundings, and surface relief characteristic of PANI is observed. The system located closer to the surface and shown in the left upper corner of the STM frame is composed of three interrupted hillocks 12.0 nm high. The width of each hill varies substantial-

TABLE 1

Parameters of thermal stability of the samples: PANI and nanocomposites PANI–Bi_2Te_3 and PANI–Bi_2Te_3–MWCNTs

Sample	T_{oII}, °C	T_m, °C	T_5, °C	T_{10}, °C	T_{30}, °C	T_{50}, °C	T_{HRI}, °C	m_r, %
PANI	166.0	470.0	81.0	228.2	370.0	433.4	124.7	5.0
PANI–Bi_2Te_3	166.0	379.0	88.0	272.3	360.1	379.3	123.1	17.1
PANI–Bi_2Te_3–MWCNTs	166.0	368.7	91.5	292.9	366.0	381.5	125.5	18.6

Notes. 1. T_{oII} – temperature corresponding to the onset of the second stage of destruction; T_m – temperature corresponding to the minimum on DTG curve; T_5, T_{10}, T_{30}, T_{50} – temperatures at which the sample mass loss is 5, 10, 30, 50 %, respectively; T_{HRI} – heat resistance index; m_r – residual sample mass after experiment. 2. PANI – polyaniline; MWCNTs – multi-walled carbon nanotubes.

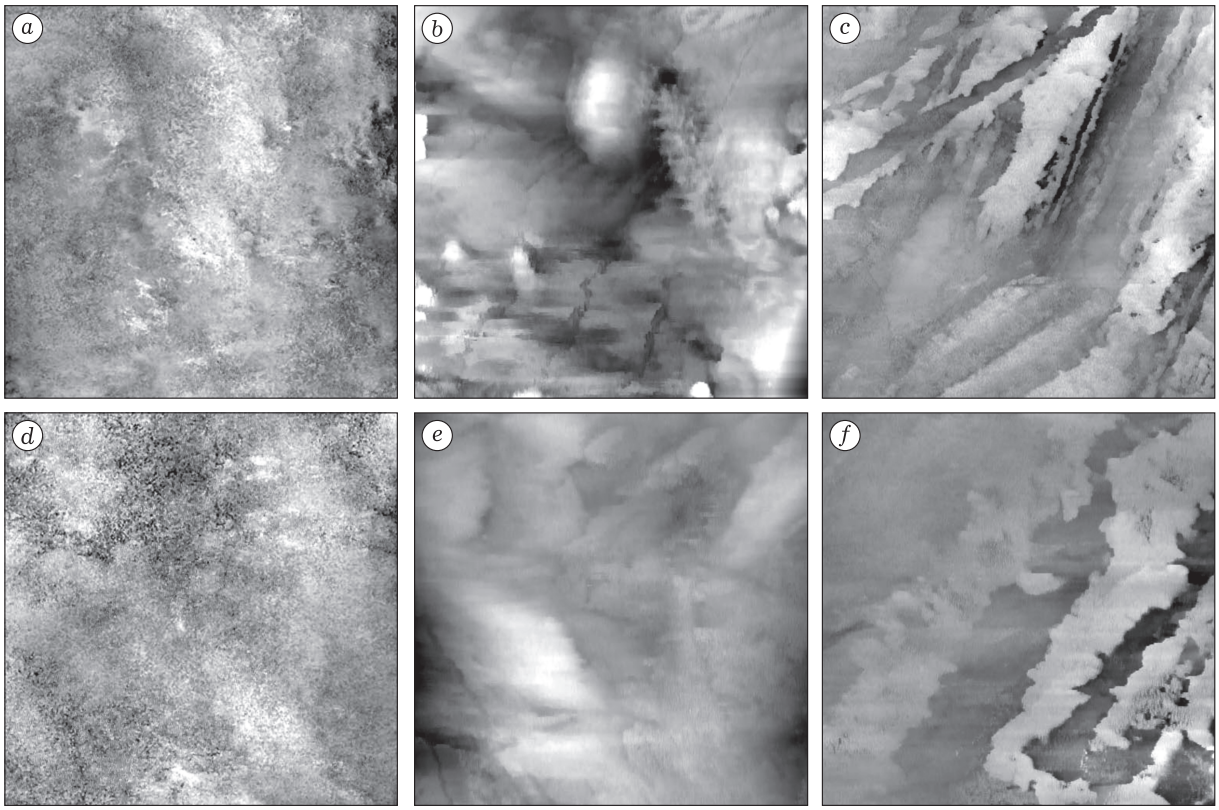

Fig. 3. Images obtained by scanning tunnelling microscopy (STM frames), the size: 1.117 × 1.117 μm (*a*–*c*), 558.3 × 558.3 nm (*d*–*f*), of sample surface with the height difference: PANI – 31.7 nm (*a*, *d*), PANI–Bi_2Te_3 – 58.2 nm (*b*, *e*), PANI–Bi_2Te_3–MWCNTs – 44.8 nm (*c*, *f*). For designations, see Fig. 2.

ly (37.0–121.0 nm), and their shapes are individually irregular and complex. The edges of hills often form semi-circles 24.0–40.0 nm in diameter (see Fig. 3, *c*, *f*), slightly going out of the hill plane (by 12.0–15.0 nm). The shape of the hills of this system indicates the presence of spherical particles, which may be Bi_2Te_3 nanoparticles coated with PANI, and the particles are localised in the direct vicinity to the extended PANI–MWCNTs structures. The third system of hillocks, represented in the upper right corner of the STM frame, is located close to the surface and is characterised by the average height of 41.0 nm. This system includes two broad (the average width being 130.0 and 106.0 nm) hills 772.7 and 600.0 nm long, a group of two closely located narrow (48.0 and 35.0 nm) and extended (533.0 nm) hills 31.7 and 23.2 nm high, and three parallel ridges of small height (10.0 nm). These irregularities are due to substantially deepened PANI–MWCNTs, complex layered structures located close to the surface, which may be PANI–MWCNTs with closely located PANI–Bi_2Te_3 particles. So, the PANI–Bi_2Te_3–MWCNTs sample is the intercalated nanocomposite: the polymer is present around each of nanophases represented in the composite, and the groups of similarly directed hills are observed, which are possibly the components of nanocomposite, MWCNTs and Bi_2Te_3, interconnected through PANI.

CONCLUSION

In the present work, the effect of nanophase on the thermal destruction of PANI–Bi_2Te_3, PANI–Bi_2Te_3–MWCNTs nanocomposites and on the specificity of the surface of tablets pressed from these nanocomposites is investigated by STA and STM. The STA data for both types of nanocomposites are to a great extent similar, but differ substantially from the data for the matrix (PANI). It is determined that the introduction of nanophase Bi_2Te_3 has a significant effect on all destructive processes in the composite, which is especially vividly pronounced on TG, DTG curves within the temperature range of the main (third) stage of destruction (230–487 °C): the mass loss by the sample accelerates dramatically within the temperature range of 326–402 °C, while the destruction of PANI proceeds slower within a broad

temperature range (219–577 °C). The introduction of MWCNTs leads to a more vigorous destruction of the nanocomposite in the region of 369 °C and to the emergence of a destructive process at the end of the third stage. A distinguishing feature of thermally stimulated processes in the nanocomposites of both types is the occurrence of the fourth stage of destruction, proceeding within the high-temperature region (at 779–977 °C), while in PANI all processes are completed at 577 °C. The introduction of the nanophase causes a decrease in mass loss at the first and third stages of thermal destruction. At the third stage, this parameter is equal to 84.7, 68.0 and 66.4 % for PANI, PANI–Bi_2Te_3 and PANI–Bi_2Te_3–MWCNTs, respectively.

It is established that the structure of nanocomposite surface is directly dependent on the composition. Analysis of the STM frames has shown that the surface relief of the PANI–Bi_2Te_3 nanocomposite is characterised by the randomly localised regions of sharply standing out hills with spherical shapes and varied height, which are not observed in the images of PANI surface. Comparison of nanoparticles sizes, determined using XRD method, with the structures observed in STM frames allows assuming that the nanoparticles possess the core-shell structure with the outer layer represented by PANI, while the inner one being Bi_2Te_3. The surface of the PANI–Bi_2Te_3–MWCNTs nanocomposite possesses radically different structure: the STM images exhibit a complex of the systems of quasi-regular hills in different directions, which are most probably the inorganic nanophase, namely MWCNTs and Bi_2Te_3, interconnected through PANI.

Acknowledgements

Authors thank the Baikal Analytical Centre at the IrIC SB RAS, the Multi-Access Centre "High-Temperature Circuit" at the Melentiev Energy Systems Institute SB RAS, and personally Cand. Sci. in Technology A. N. Kozlov for having provided the data of synchronous thermal analysis of our samples.

REFERENCES

1 Kwan T. H., Wu X., Yao Q., Complete implementation of the combined TEG-TEC temperature control and energy harvesting system, *Control Eng. Pract.*, 2020, Vol. 95, Art. 104224.
2 Khan S., Kim J., Acharya S., Kim W., Review on the operation of wearable sensors through body heat harvesting based on thermoelectric devices, *Appl. Phys. Lett.*, 2021, Vol. 118, No. 20, Art. 200501.
3 Nozariasbmarz A., Collins H., Dsouza K., Polash M. H., Hosseini M., Hyland M., Liu J., Malhotra A., Ortiz F. M., Mahaddes F., Ramesh V. P., Sargolzaeiaval Y., Snouwaert N., Özturk M. C., Vashaee D., Review of wearable thermoelectric energy harvesting: from body temperature to electronic systems, *Appl. Energy.*, 2020, Vol. 258, Art. 114069.
4 Hou Y., Yang Y., Wang Z., Li Z., Zhang X., Bethers B., Xiong R., Guo H., Yu H., Whole fabric-assisted thermoelectric devices for wearable electronics, *Adv. Sci.*, 2022, Vol. 9, No. 1, Art. 2103574.
5 Zhang P., Deng B., Sun W., Zheng Z., Liu W., Fiber-based thermoelectric materials and devices for wearable electronics, *Micromachines*, 2021, Vol. 12, No. 8, Art. 869.
6 Mata-Padilla J. M., Ávila-Orta C. A., Cruz-Delgado V. J., Martínez-Colunga J. G., Nanostructured polymers for thermoelectric conversion, in: Handbook of Nanomaterials and Nanocomposites for Energy and Environmental Applications, O. V. Kharissova, L. M. Torres-Martínez, B. I. Kharisov (Eds.), Springer, Cham, 2021, P. 3393–3419.
7 Na Y., Kim S., Mallem S. P. R., Yi S., Kim K. T., Park K. I., Energy harvesting from human body heat using highly flexible thermoelectric generator based on Bi_2Te_3 particles and polymer composite, *J. Alloys Compd.*, 2022, Vol. 924, Art. 166575.
8 Jin H., Li J., Iocozzia J., Zeng X., Wei P.-C., Yang C., Li N., Liu Z., He H., Zhu T., Wang J., Lin Z., Wang S., Hybrid organic-inorganic thermoelectric materials and devices, *Angew. Chem. Int. Ed.*, 2019, Vol. 58, No. 43, P. 15206–15226.
9 Idumah C. I., Novel trends in conductive polymeric nanocomposites, and bionanocomposites, *Synth. Met.*, 2021, Vol. 273, Art. 116674.
10 Liu S., Li H., Li P., Liu Y., He C., Recent advances in polyaniline-based thermoelectric composites, *CCS Chem.*, 2021, Vol. 3, No. 10, P. 2547–2560.
11 Khan J. S., Akram R., Hussain M., Rafique S., Kayani F. B., Rehman A. U., Thermoelectric properties of polyvinylpyrrolidone/polyaniline-mixed Bi_2Te_3 composites prepared by electrospinning, *Polym. Compos.*, 2023, Vol. 44, No. 5, P. 2745–2756.
12 Wang Y., Yu C., Sheng M., Song S., Deng Y., Individual adjustment of electrical conductivity and thermopower enabled by multiple interfaces in polyaniline-based ternary hybrid nanomaterials for high thermoelectric performances, *Adv. Mater. Interfaces*, 2018, Vol. 5, No. 10, Art. 1701168.
13 Blackburn J. L., Ferguson A. J., Cho C., Grunlan J. C., Carbon-nanotube-based thermoelectric materials and devices, *Adv. Mater.*, 2018, Vol. 30, No. 11, Art. 1704386.
14 Zhang C., Li H., Liu Y., Li P., Liu S., He C., Advancement of polyaniline/carbon nanotubes based thermoelectric composites, *Materials*, 2022, Vol. 15, No. 23, Art. 8644.
15 Zhmurova A. V., Prozorova G. F., Zvereva M. V., Mechanochemical synthesis and DC electrical conductivity of PANI-based MWCNT containing nanocomposites with Te^0 and Bi_2Te_3 thermoelectric nanophase, *Powders*, 2023, Vol. 2, No. 3, P. 540–561.
16 Qi Y.-N., Xu F., Ma H.-J., Sun L.-X., Zhang J., Jiang T., Thermal stability and glass transition behavior of PANI/γ-Al_2O_3 composites, *J. Therm. Anal. Calorim.*, 2008, Vol. 91, No. 1, P. 219–223.
17 Palaniappan S., Narayana B. H., Temperature effect on conducting polyaniline salts: thermal and spectral studies, *J. Polym. Sci., Part A: Polym. Chem.*, 1994, Vol. 32, No. 13, P. 2431–2436.
18 Mota M. L., Carrillo A., Verdugo A. J., Olivas A., Guerrero J. M., de la Cruz E. C., Noriega Ramírez N., Synthesis and novel purification process of PANI and PANI/AgNPs composite, *Molecules*, 2019, Vol. 24, No. 8, Art. 1621.

19 Ma C., Yang Z., Wang W., Zhang M., Hao X., Zhu S., Chen S., Fabrication of Ag–Cu_2O/PANI nanocomposites for visible-light photocatalysis triggering super antibacterial activity, *J. Mater. Chem. C*, 2020, Vol. 8, No. 8, P. 2888–2898.
20 Rashid M., Islam M. M., Minami H., Aftabuzzaman M., Rahman M. A., Hossain M. M., Hoque S. M., Alam M. A., Ahmad H., Nickel decorated melamine-formaldehyde resin/polyaniline composites for high specific capacitance, *Mater. Chem. Phys.*, 2020, Vol. 249, Art. 122957.
21 Venkateshaiah A., Padil V. V. T., Nagalakshmaiah M., Waclawek S., Černík M., Varma R. S., Microscopic techniques for the analysis of micro and nanostructures of biopolymers and their derivatives, *Polymers*, 2020, Vol. 12, No. 3, Art. 512.
22 Zhang C., Yi Z., Xu W., Scanning probe microscopy in probing low-dimensional carbon-based nanostructures and nanomaterials, *Materials Futures*, 2022, Vol. 1, No. 3, Art. 032301.
23 Hong J., Bekyarova E., Liang P., de Heer W. A., Haddon R. C., Khizroev S., Room-temperature magnetic ordering in functionalized grapheme, *Sci. Rep.*, 2012, Vol. 2, No. 1, Art. 624.
24 Bahramnia H., Semnani H. M., Habibolahzadeh A., Abdoos H., Epoxy/polyurethane hybrid nanocomposite coatings reinforced with MWCNTs and SiO_2 nanoparticles: processing, mechanical properties and wear behavior, *Surf. Coat. Technol.*, 2021, Vol. 415, Art. 127121.
25 Namazi H., Dadkhah A., Mosadegh M., New biopolymer nanocomposite of starch-graft polystyrene/montmorillonite clay prepared through emulsion polymerization method, *J. Polym. Environ.*, 2012, Vol. 20, No. 3, P. 794–800.
26 Mallakpour S., Khadem E., A green route for the synthesis of novel optically active poly(amide–imide) nanocomposites containing *N*-trimellitylimido-*L*-phenylalanine segments and modified alumina nanoparticles, *High Perform. Polym.*, 2014, Vol. 26, No. 4, P. 392–400.
27 Qi Y.-N., Xu F., Sun L.-X., Thermal stability and glass transition behavior of PANI/MWNT composites, *J. Therm. Anal. Calorim.*, 2008, Vol. 94, No. 1, P. 137–141.
28 Kumar A. M., Gasem Z. M., Effect of functionalization of carbon nanotubes on mechanical and electrochemical behavior of polyaniline nanocomposite coatings, *Surf. Coat. Technol.*, 2015, Vol. 276, P. 416–423.
29 Rostami A., Masoomi M., Fayazi M. J., Vahdati M., Role of multiwalled carbon nanotubes (MWCNTs) on rheological, thermal and electrical properties of PC/ABS blend, *RSC Adv. 2015*, Vol. 5, No. 41, P. 32880–32890.
30 Encyclodedia of Polymers, Vol. 3, Sov. Entsykl., 1977. (In Russ.).
31 Guo Y., Xu G., Yang X., Ruan K., Ma T., Zhang Q., Gu J., Wu Y., Liu H., Guo Z., Significantly enhanced and precisely modeled thermal conductivity in polyimide nanocomposites with chemically modified graphene via *in situ* polymerization and electrospinning-hot press technology, *J. Mater. Chem. C.*, 2018, Vol. 6, No. 12, P. 3004–3015.